Atlantic Equatorial Deep Jets in Argo Float Data

SWANTJE BASTIN,[a] MARTIN CLAUS,[a,b] PETER BRANDT,[a,b] AND RICHARD J. GREATBATCH[a,b]

[a] *GEOMAR Helmholtz Centre for Ocean Research Kiel, Kiel, Germany*
[b] *Faculty of Mathematics and Natural Sciences, Kiel University, Kiel, Germany*

(Manuscript received 1 July 2021, in final form 5 March 2022)

ABSTRACT: Equatorial deep jets (EDJ) are zonal currents along the equator in all three ocean basins that alternate in direction with depth and time. In the Atlantic Ocean below the thermocline, they are the dominant variability on interannual time scales. Observations of equatorial deep jets are available but scarce, given the EDJs' location at depth, their small vertical scale, and their long periodicity of several years. In the last few years, Argo floats have added a significant number of measurements at intermediate depth. In this study we therefore revise estimates of the EDJ scales based on Argo float data. Mostly, we use velocity data at 1000-m depth calculated from float displacement, which yield robust estimates of the Atlantic EDJ period (4.6 yr), amplitude distribution, phase distribution, zonal wavelength (146.7°), and meridional structure. We also show that the equatorial amplitude of the EDJs' first meridional mode Rossby wave component (9.8 cm s^{-1}) is larger than that of their Kelvin wave component (2.8 cm s^{-1}). In addition, we present a new estimation of the EDJs' vertical structure throughout the Atlantic basin, based on an equatorial geostrophic velocity reconstruction from hydrographic Argo float measurements from depths between 400 and 2000 m. Our new estimates from Argo float data provide the first basinwide assessment of the Atlantic EDJ scales, as well as having smaller uncertainties than estimates from earlier studies.

KEYWORDS: Currents; Kelvin waves; Rossby waves; Jets; Interannual variability; Tropical variability

1. Introduction

The circulation in the tropical oceans is characterized by energetic zonal currents. Below the thermocline, there are two main current systems with flow speeds of up to 20 cm s^{-1}: one takes the form of zonal jets alternating in direction with latitude [sometimes called the Equatorial Intermediate Current System (EICS; e.g., Ascani et al. 2010) or extra-equatorial jets (EEJ; e.g., Cravatte et al. 2012, 2017; Ménesguen et al. 2019; Delpech et al. 2020b, 2021)], which are characterized by a large vertical scale and extend to at least 15°N/S. The other consists of vertically alternating, downward-propagating zonal jets that are located directly on the equator with small latitudinal extent; these are called equatorial deep jets (EDJ; e.g., Luyten and Swallow 1976; Hayes and Milburn 1980; Leetmaa and Spain 1981; Eriksen 1982; Youngs and Johnson 2015; Ménesguen et al. 2019). It is not entirely clear whether these current systems merely coexist separately in the equatorial oceans, or whether they share a common dynamical origin. So far, however, no attempt at a unified theory of their generation mechanisms has been successful (Ménesguen et al. 2019). Because of their large vertical extent and their temporal consistency, the EICS can be easily seen in time-mean velocity data derived from Argo float measurements and have also been well studied from shipboard measurement sections (e.g., Cravatte et al. 2012, 2017). Of the EDJ, however, we have a less clear picture, mainly because of their vertical and temporal variability.

Equatorial deep jets were first identified in the Indian Ocean (Luyten and Swallow 1976), and later also in the Pacific and Atlantic Oceans (Hayes and Milburn 1980; Leetmaa and Spain 1981; Eriksen 1982). They take the form of stacked zonal jets with downward phase propagation and, consistent with linear wave theory, exhibit upward energy propagation in an idealized model simulation (Matthießen et al. 2015). Associated with the latter, the EDJ in the Atlantic Ocean have been suggested to influence surface climate parameters like wind, rainfall, and sea surface temperature on interannual time scales (Brandt et al. 2011), potentially making the EDJ important for seasonal to interannual prediction in the equatorial regions. Furthermore, the comparably fast-flowing jets advect tracers, and have been shown to contribute to the ventilation of the eastern tropical oxygen minimum zones from the highly oxygenated western boundary region (Brandt et al. 2012, 2015). In addition to this, the EDJ have been suggested to generate time-mean zonal flow by nonlinear self-advection (Ascani et al. 2015; Bastin et al. 2020), which is relevant to, e.g., nutrient and oxygen transport in the deep ocean.

Given the EDJs' relatively small vertical scale of a few hundred meters and their temporal variability on time scales of multiple years, it is challenging to observe them. Their vertical wavelength of a few hundred meters and their amplitude of

Denotes content that is immediately available upon publication as open access.

Supplemental information related to this paper is available at the Journals Online website: https://doi.org/10.1175/JPO-D-21-0140.s1.

Bastin's current affiliation: Max Planck Institute for Meteorology, Hamburg, Germany.

Corresponding author: Swantje Bastin, swantje.bastin@mpimet.mpg.de

DOI: 10.1175/JPO-D-21-0140.1

up to 20 cm s^{-1} at specific locations have been among the first parameters that could be estimated, from several instantaneous shipboard velocity profiles or sections (e.g., Luyten and Swallow 1976; Leetmaa and Spain 1981; Ponte et al. 1990; Gouriou et al. 1999). Later, concurrent measurements at different longitudes showed that the EDJ are zonally coherent over several tens of degrees (Gouriou et al. 2001). Johnson et al. (2002) then combined historical CTD measurements from the equatorial Pacific to extract information on the Pacific EDJ and found a slow temporal evolution; but concluded that the period of the Pacific EDJ must be significantly longer than the time span where measurements were available. A similar analysis by Johnson and Zhang (2003) in the Atlantic yielded not only information about the period, which they estimated to be 5 ± 1 yr, but also about the meridional structure of the Atlantic EDJ, which they described as roughly corresponding to the meridional structure of a first meridional mode Rossby wave, widened by a factor of 1.5 relative to that expected based on inviscid theory. The temporal variation of the EDJ subsequently became better known due to the usage of moored current meters to obtain time series of velocity measurements (e.g., Bunge et al. 2006, 2008; Brandt et al. 2008). Especially useful in this context is the equatorial mooring at 23°W, having provided high-resolution velocity measurements since 2006, and being still maintained today. This moored velocity dataset has been used in a number of studies concerned with the EDJ and has given a thorough insight into the Atlantic EDJs' temporal and vertical structure in the center of the basin (Brandt et al. 2008, 2011, 2012; Claus et al. 2016; Greatbatch et al. 2018). The latest analysis of the basinwide signature of the EDJ has been provided by Youngs and Johnson (2015), who did an updated analysis of available shipboard CTD profiles for all three oceans (for the Indian and Pacific Ocean they also included Argo profiles). They supplied updated estimates of temporal and vertical scales, but also of the meridional structure and zonal wavelength of the EDJ, albeit still with sizeable uncertainties and as basinwide averages. However, as we will show in this study, the amplitude, zonal wavelength, and meridional structure of the Atlantic EDJ exhibit pronounced horizontal variations within the basin.

Dynamically, the EDJ have been suggested to originate from an instability of intraseasonal waves (Hua et al. 2008) shed either by tropical instability waves (Ascani et al. 2015) or by the western boundary currents (d'Orgeville et al. 2007). The strong similarity of the EDJ to a resonant equatorial basin mode (Cane and Moore 1981) for a high baroclinic mode has been noted by several studies (e.g., d'Orgeville et al. 2007; Ascani et al. 2015; Matthießen et al. 2015, 2017), although they are broader than theoretically expected, possibly because of enhanced momentum relative to tracer dissipation in the equatorial ocean (Greatbatch et al. 2012). Equatorial basin modes consist of an eastward-propagating equatorial Kelvin wave, together with its reflection as westward-propagating long equatorial Rossby waves: the sum of these waves becomes resonant, for the gravest basin mode, at a period equivalent to 4 times the time it takes the Kelvin wave to cross the entire basin (Cane and Moore 1981). Because of this dependence on the basin width, the time scale on which the Pacific EDJ vary has been found to be much longer than that of the Atlantic and Indian Ocean EDJ (e.g., Youngs and Johnson 2015). The nature of the EDJ as a resonant sum of multiple wave components of course complicates their structure. Although Cane and Moore (1981) have provided analytic solutions to the equatorial basin modes, these are only for a linear idealized ocean, leaving it unclear what exact form they would take in the real ocean including nonlinear effects and dissipation. In several studies, especially the early ones that only had access to a very limited number of measurements, attempts have been made to attribute the EDJ variability either to an equatorial Kelvin wave or to equatorial Rossby waves, leading to conflicting results. Youngs and Johnson (2015) provided combined estimates of the contributions of the Kelvin and Rossby waves to the EDJ and concluded that in the Indian and Pacific Oceans, the two are of similar importance, whereas the Atlantic EDJ seem to be dominated by the first meridional mode Rossby wave.

With this study, we provide an updated, independent, more accurate and comprehensive description of the EDJ using the growing amount of data from the deep equatorial oceans provided by Argo floats. The Argo program has, since its beginning in 1998, brilliantly fulfilled its original aim to provide worldwide real-time measurements of temperature and salinity (in later years also additional parameters like, e.g., oxygen) from the upper 2000 m of the oceans. Through its implementation of a global network of autonomous measuring floats, it has now provided a much larger number of hydrographic profiles than shipboard measurements, and at a much lower cost (Jayne et al. 2017). In the equatorial oceans, the number of available Argo float measurements has increased especially in the last 5–10 years—these data now give us the chance to compile a more comprehensive basinwide description of the EDJ than available so far. However, we can provide this only for the Atlantic Ocean: It has been found before that the Atlantic EDJ are stronger and more regular than those in the Pacific and Indian Oceans (e.g., Youngs and Johnson 2015), a finding that is supported by the analysis of velocity data at 1000-m depth presented in this study. In fact, in this data, we were not able to detect the Indian and Pacific Ocean EDJ, such that the focus of this article will be on the Atlantic EDJ only.

This article is structured as follows: section 2 describes the datasets and analysis methods that were used. In section 3, we present our estimation of 1) the Atlantic EDJs' frequency, 2) their amplitude, 3) their phase and zonal wavelength, 4) their meridional structure and the relative contributions of Kelvin and Rossby waves to the EDJ signal, and 5) the Atlantic EDJs' vertical structure. The results are then summarized and discussed in section 4.

2. Data and methods

a. Data

1) Velocity data at 1000-m depth

The main dataset that we used for this study is the YoMaHa'07 dataset of "velocity data assessed from trajectories of Argo floats at parking level and at the sea surface"

(Lebedev et al. 2007). The deep velocity dataset is composed of one (zonal and meridional) velocity value at the parking depth per Argo float cycle consisting of a descent to the parking depth, a floating period at this depth, and an ascent back to the surface. The velocities have been estimated from the float location before descent and after ascent, and the time spent at depth; thus they are not instantaneous velocities but averages over typically around ten days (Lebedev et al. 2007). For the analysis of equatorial deep jets, this should not pose a problem, because the interest is on much longer time scales such that the information that is lost through the average would merely be regarded as noise in the context of this study. The YoMaHa'07 dataset is updated regularly; the data that we used were obtained online (http://apdrc.soest.hawaii.edu/projects/Argo/data/trjctry/yomaha07.dat.gz) on 1 July 2020 and extend to June 2020.

From this dataset, we only used data from the equatorial oceans and restricted the analysis to data from floats with a nominal parking depth of 1000 m, because at this depth the data are most abundant. Although there are some Argo floats that dive to other parking depths, e.g., 500 or 2000 m, these are so few today that, at least concerning the EDJ, no meaningful statistical analysis is possible.

In Fig. 1, the zonal velocity along the equator at 1000-m depth is shown for the Atlantic Ocean. Especially since 2014, the data coverage shows a pronounced increase at this depth. Overall, almost 85 000 zonal velocity data points are available and used in our analyses from the YoMaHa'07 dataset between 2000 and June 2020, at 1000-m depth, in the Atlantic Ocean between 4°S and 4°N. The YoMaHa'07 dataset is used for the estimation of all Atlantic EDJ parameters except their vertical wavelength.

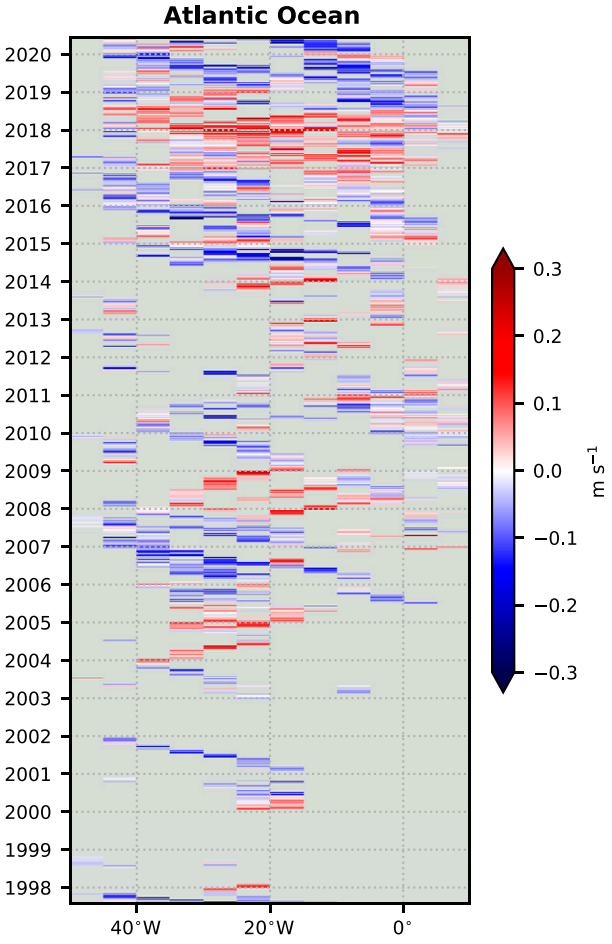

FIG. 1. Hovmöller diagram of zonal velocity at 1000-m depth along the equator in the Atlantic Ocean, from the YoMaHa'07 dataset (Lebedev et al. 2007). The shown zonal velocity values are averages between 1°S and 1°N and over 5° longitude bins. Positive values mean eastward velocity; negative values indicate westward velocity.

2) HYDROGRAPHIC DATA

Because the Argo floats do not measure velocity directly (making it necessary to calculate the velocity indirectly from their travel time and displacement at depth), the YoMaHa'07 deep velocity dataset only contains data points at the floats' parking depth and therefore does not allow us to examine the EDJs' vertical structure. However, the Argo floats directly measure hydrographic parameters during their descent and/or ascent, making it possible to compute the instantaneous vertical structure of the density field. Because the zonal velocity associated with the EDJ is almost entirely in geostrophic balance (Eriksen 1982), the density field contains information about the vertical structure of the Atlantic EDJ.

We used all available Argo float profiles from the equatorial Atlantic, from January 2001 to June 2020 (Argo 2020). From these, we used the temperature, salinity, and pressure data to calculate the in situ density using a Python implementation of the Gibbs seawater library (*gsw 3.3.1*). If, from the variable in question, the "_ADJUSTED" version was present (meaning changes have been made to the raw data as part of quality control), we used it, otherwise we used the original, unchanged version. All values were checked in terms of their quality flags; only values flagged as *good data*, *probably good data*, *value changed*, or *estimated value* were used (cf. Argo Data Management Team 2019, p. 69). We did not limit our analysis to delayed-mode (or D-mode) profiles: we included also real-time or raw (R-mode) and real-time adjusted (A-mode) profiles as long as their quality flags indicated good quality data. However, D-mode data represent the largest part of the profiles that we used (68% of about 60 000 profiles between 2001 and 2020, in the Atlantic between 2°S and 2°N). We included also A- and R-mode data because although the largest percentage of the used data are D-mode data, the data availability decreases a lot when only using D-mode data. The reason for this is that we use the hydrographic Argo data to calculate the second meridional derivative of density, $\partial^2\rho/\partial y^2$. This requires three density measurements to get one data point, and if only one of them is not D-mode data, we lose the data point. However, there seemed to be no quality differences between the $\partial^2\rho/\partial y^2$ profiles including A- and R-mode data and those from only D-mode data.

Figure S1 in the online supplemental material shows the second meridional derivative of the in situ density, $\partial^2\rho/\partial y^2$,

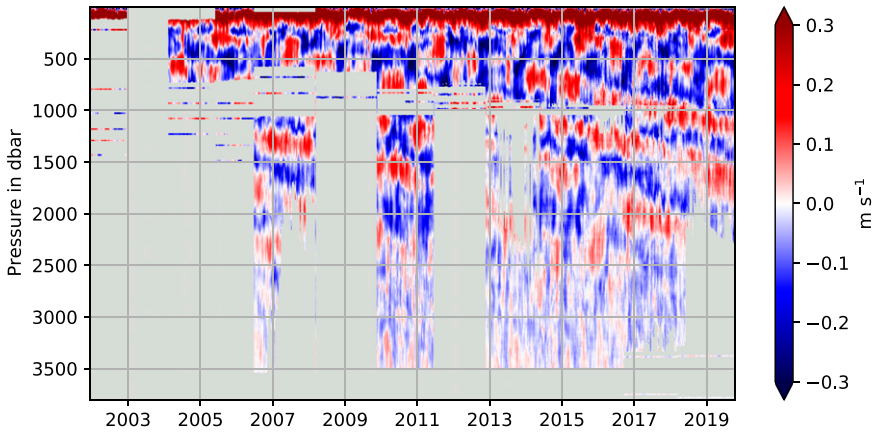

FIG. 2. Equatorial zonal velocity at 23°W measured by moored current meters [updated from, e.g., Greatbatch et al. 2018)]. Positive values indicate eastward velocity; negative values indicate westward velocity.

estimated from the equatorial Atlantic Argo float profiles between 1°S and 1°N wherever possible, otherwise between 2°S and 2°N [for details on the relation between the EDJ and $\partial^2\rho/\partial y^2$, see section 2b(4)]. Indeed, EDJ-like structures are visible at all longitudes shown in Fig. S1, as can be seen from a cursory comparison with Fig. 2.

3) VALIDATION DATASET

The Atlantic EDJ characteristics have been estimated multiple times from the extensive deep velocity dataset from moored current meters at 23°W (Bunge et al. 2008; Brandt et al. 2011; Claus et al. 2016; Greatbatch et al. 2018). We want to use this dataset as an independent measurement of the EDJ to validate the parameters that we estimate from the Argo float data. Rather than just comparing our estimates with those from other studies, we use an updated version (extending to October 2019) here to get more robust estimates of the parameters. The vertical resolution of the mooring data depends on the used instruments as well as on data gaps between the measurement range of the instruments. We use a dataset that has been interpolated to 1-dbar vertical resolution. A detailed description of the dataset and measurement methods can be found in Tuchen et al. (2018). The equatorial zonal velocity measured by the moored instruments at 23°W is shown in Fig. 2 [updated from, e.g., Greatbatch et al. (2018)].

b. Analysis methods

1) DETECTION OF PERIODIC SIGNALS: LOMB–SCARGLE PERIODOGRAMS

To detect the periodic signal of the EDJ, both in time and space, we used the Lomb–Scargle periodogram (cf. Lomb 1976; Scargle 1982). This is a useful method of detecting periodicity in cases where Fourier transformation cannot be applied because of uneven sampling or missing data. Calculating the Lomb–Scargle periodogram is equivalent to least squares fitting of sine waves to the data for a given set of frequencies (Scargle 1982). The periodogram is given by the explained variance of the least squares sine fit for each frequency. By normalizing with the number of observations N, an estimate of the power spectrum P_{pow} can be obtained [as well as the amplitude spectrum, which is then $P_{\mathrm{amp}} = (P_{\mathrm{pow}})^{1/2}$]:

$$P_{\mathrm{pow}}(f) = \frac{\sum_{j=1}^{N}[X(t_j)]^2 - \sum_{j=1}^{N}[X(t_j) - X_f(t_j)]^2}{N^2}, \qquad (1)$$

where $X(t_j)$ are the data points and $X_f(t_j)$ is the value of the fitted sine wave at time t_j for frequency f. For evenly spaced data, the result will be equal to the power spectrum obtained by Fourier transformation, if the frequencies for the sine wave fits are chosen accordingly.

2) SPATIAL SMOOTHING

Because the data are relatively sparse even at 1000-m depth, some spatial smoothing of the Argo velocity data is done with a 2D Gaussian filter, following Bastin et al. (2020). For this, we first bin the YoMaHa'07 data onto a fine grid ($0.1° \times 0.1° \times 7$ days), and then apply the filter. To make sure that we do not average over scales that are larger than the scales on which the zonal velocity field can be assumed to be coherent, we choose the filter scales based on the decorrelation scales of the zonal velocity at 1000-m depth. Based on the spatial autocorrelation of the zonal velocity field, which is shown in Fig. 3, the zonal decorrelation scale of the zonal velocity is approximately 10° and the meridional decorrelation scale is approximately 0.4°. For the filter scales, we choose 7.5° in the zonal direction and 0.3° in the meridional direction, to stay below the estimated decorrelation scales. For more details see the supporting information of Bastin et al. (2020).

3) UNCERTAINTY QUANTIFICATION

We used bootstrapping to obtain uncertainties for our parameter estimations. Bootstrapping allows us to determine confidence intervals for estimated parameters without prior knowledge of the shape of the underlying distribution (e.g.,

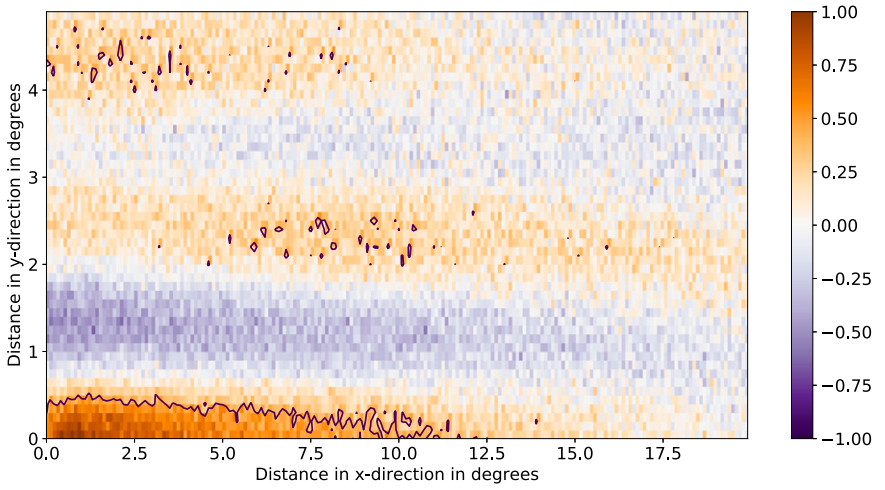

FIG. 3. Spatial decorrelation scales of time-mean zonal velocity at 1000-m depth in the tropical Atlantic Ocean between 7°S and 7°N. The color shading shows the autocorrelation, and the black contour at a value of 0.37 indicates the *e*-folding scale. [This figure is a reproduction of Fig. S3 in Bastin et al. (2020).]

Efron 1979). For each parameter of the Atlantic EDJ that we estimate, we take 10 000 resample sets (with replacement and equal probability for each point to be selected) of the original unsmoothed and unbinned dataset used to estimate the parameter, then calculate the parameter again (including bin-averaging and all other analysis steps) from each of these resample sets, such that we get a distribution for the parameter in question. The sample size of each of the 10 000 resample sets is the same as the sample size available from the original data. We preserve the time and space information of each data point when resampling, such that the data are not shuffled in time or space, but some data points are omitted or included multiple times. From the resulting distribution of values for the parameter in question, we then give a 95% confidence interval by taking the 2.5% and 97.5% quantiles. This method can give a measure of the error in our parameter estimation connected to sampling uncertainties. Additional errors, especially of a systematic kind, originating, e.g., from measurement errors, are not considered.

4) ESTIMATION OF VERTICAL EDJ SCALE FROM HYDROGRAPHIC DATA

We make use of the fact that the EDJ are, approximately, in geostrophic balance (e.g., Eriksen 1982) to extract information about their vertical scale from the hydrographic data provided by the Argo floats. At the equator, the geostrophic balance for the zonal flow takes the form

$$\beta u = -\frac{1}{\rho_0}\frac{\partial^2 p}{\partial y^2} \quad \text{for} \quad y \to 0, \tag{2}$$

where $\beta = df/dy$ is the meridional derivative of the Coriolis parameter, u is the zonal velocity, ρ_0 is a constant reference density, p is the pressure, and y indicates distance from the equator measured positive northward (e.g., Gill 1982, p. 461).

We can relate the geostrophic velocity to the density field by using the hydrostatic balance

$$-\rho g = \partial p/\partial z, \tag{3}$$

where ρ is the (variable) in situ density, g is the gravitational acceleration, p is the pressure, and z is the water depth measured positive upward. Combining Eqs. (2) and (3) leads to the equatorial form of the thermal wind equation:

$$\beta\frac{\partial u}{\partial z} = \frac{g}{\rho_0}\frac{\partial^2 \rho}{\partial y^2} \tag{4}$$

or, if using the pressure as vertical coordinate [with $\partial z/\partial p$ from Eq. (3)],

$$\frac{\partial u}{\partial p} = -\frac{1}{\beta\rho_0\rho}\frac{\partial^2 \rho}{\partial y^2}. \tag{5}$$

It is thus possible to reconstruct the equatorial geostrophic velocity field from the density field, provided that we know the velocity at some reference pressure p_{ref}, as

$$u(p) = -\frac{1}{\beta\rho_0}\int_{p_{\text{ref}}}^{p}\left(\frac{1}{\rho}\frac{\partial^2 \rho}{\partial y^2}\right)dp' + u(p_{\text{ref}}). \tag{6}$$

As reference velocity, we use the YoMaHa'07 data at a pressure of 1000 dbar.

5) STRETCHING OF VERTICAL COORDINATE

The stratification of the water column affects the vertical wavelength and the amplitude of waves propagating through it. To correct for this effect when analyzing the vertical

structure of the Atlantic EDJ, we apply scaling and stretching corresponding to the Wentzel–Kramers–Brillouin–Jeffreys (WKBJ) approximation (Gill 1982). We stretch the vertical pressure coordinate p as described in Leaman and Sanford (1975):

$$dp^* = \frac{\overline{N}(p)}{N_0} dp, \tag{7}$$

where p^* denotes stretched pressure. The zonal velocity u has been scaled, again following Leaman and Sanford (1975), as

$$u^*(p) = u(p)\left[\frac{N_0}{\overline{N}(p)}\right]^{1/2}. \tag{8}$$

The $\overline{N}(p)$ denotes a typical profile of the Brunt–Väisälä frequency N, and N_0 denotes the vertical average of $\overline{N}(p)$. Following Youngs and Johnson (2015), we calculated $\overline{N}(p)$ as the horizontally and temporally averaged N from hydrographic Argo data from the region of interest, in our case the equatorial Atlantic, with no restriction on longitude, between 1°S and 1°N and between 400- and 2000-m depth. In addition, $\overline{N}(p)$ has been smoothed vertically using a Hanning filter with a half-width of 200 dbar as in Youngs and Johnson (2015). The resulting $\overline{N}$ and N_0 can be seen in Fig. 4 and are provided online together with the analysis scripts (see the data availability statement for the links).

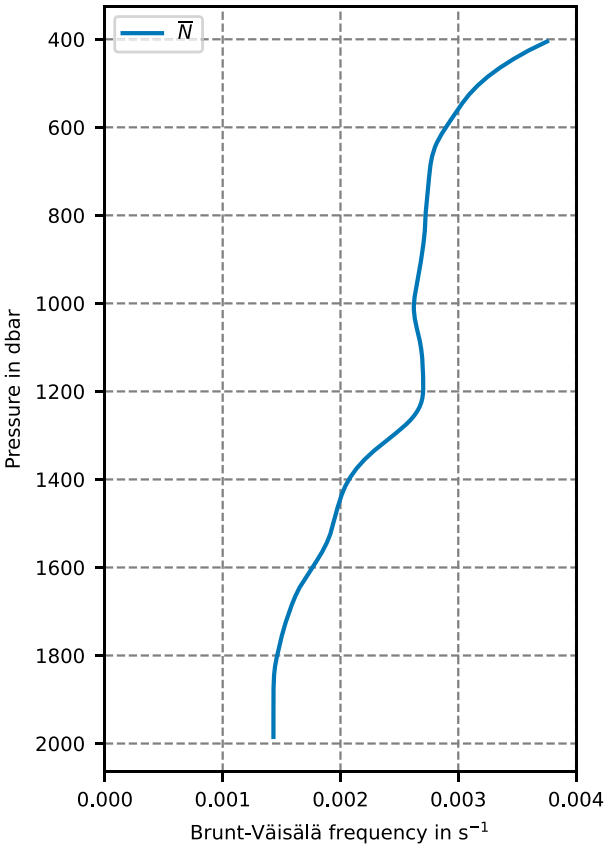

FIG. 4. Stratification profile used for vertical WKBJ stretching and scaling. The vertical average of the $\overline{N}$ profile shown in the figure is $N_0 = 2.35 \times 10^{-3}$ s^{-1}. The data are provided as an additional dataset (see the data availability statement for the link).

3. Results

a. *Frequency at 1000-m depth*

In Fig. 1, a Hovmöller diagram of the equatorial zonal velocity at 1000-m depth in the Atlantic from the YoMaHa'07 deep velocity dataset is shown. The velocity values are averaged between 1°S and 1°N, as well as over 5° longitude bins. The EDJ are visible as interannual variation of the zonal velocity, propagating from the eastern boundary toward the west, which also appears to be the strongest signal in the data. This is corroborated by the power spectrum of equatorial zonal velocity at 1000-m depth, again averaged between 1°S and 1°N and over 5° longitude bins, which is shown in Fig. 5a. Since the EDJs' phase is not constant throughout the basin but depends on the longitude, separate Lomb–Scargle periodograms for each 5° longitude bin have been computed and are shown in Fig. 5a as colored lines. The average of all these spectra is shown as the dashed black line. The Lomb–Scargle periodograms have been calculated at frequencies with a resolution of 2×10^{-4} yr^{-1}. Indeed, the interannual peak associated with the EDJ at a period of 4.60 yr is the most energetic signal in the zonal velocity at 1000-m depth in the equatorial Atlantic. Additionally, a somewhat weaker annual signal can be seen, as well as an even weaker semiannual peak. This fits well to previous estimates from the 23°W mooring (Claus et al. 2016; Greatbatch et al. 2018), although in these studies the annual peak appears stronger than the interannual peak, because variability at all depths instead of only 1000 m has been included in the analysis. The annual and semiannual cycles in the Atlantic Ocean are dominantly associated with the fourth and second baroclinic mode, respectively, as shown by Brandt et al. (2016), so the amplitude will show a strong dependence on depth. The location of the interannual peak in the spectrum is consistent over all the periodograms, meaning that the time scale of the Atlantic EDJ is independent of longitude, as we would expect from their theoretical explanation as a resonant basin mode (Greatbatch et al. 2012). The 95% confidence interval from bootstrapping is found to be between 0.2156 and 0.2192 yr^{-1}, shown in Fig. 5b, corresponding to the period range between 4.64 and 4.56 yr. Note that the periods are calculated as the reciprocal of the frequency values and not from an independent estimation via bootstrapping. All parameter estimates described in this paper are summarized in Table 1.

In Fig. 5c, a comparison with the EDJ frequency estimated from the 23°W mooring dataset is shown, as well as a comparison with the depth-independent estimate from frequency-vertical wavenumber spectra by Youngs and Johnson (2015). The mooring data have been binned to a vertical resolution of 10 dbar, after which a Lomb–Scargle periodogram has been calculated for each depth and the frequency of the interannual peak has been detected. The estimate from the YoMaHa'07 velocity data at 1000-m depth lies well within the

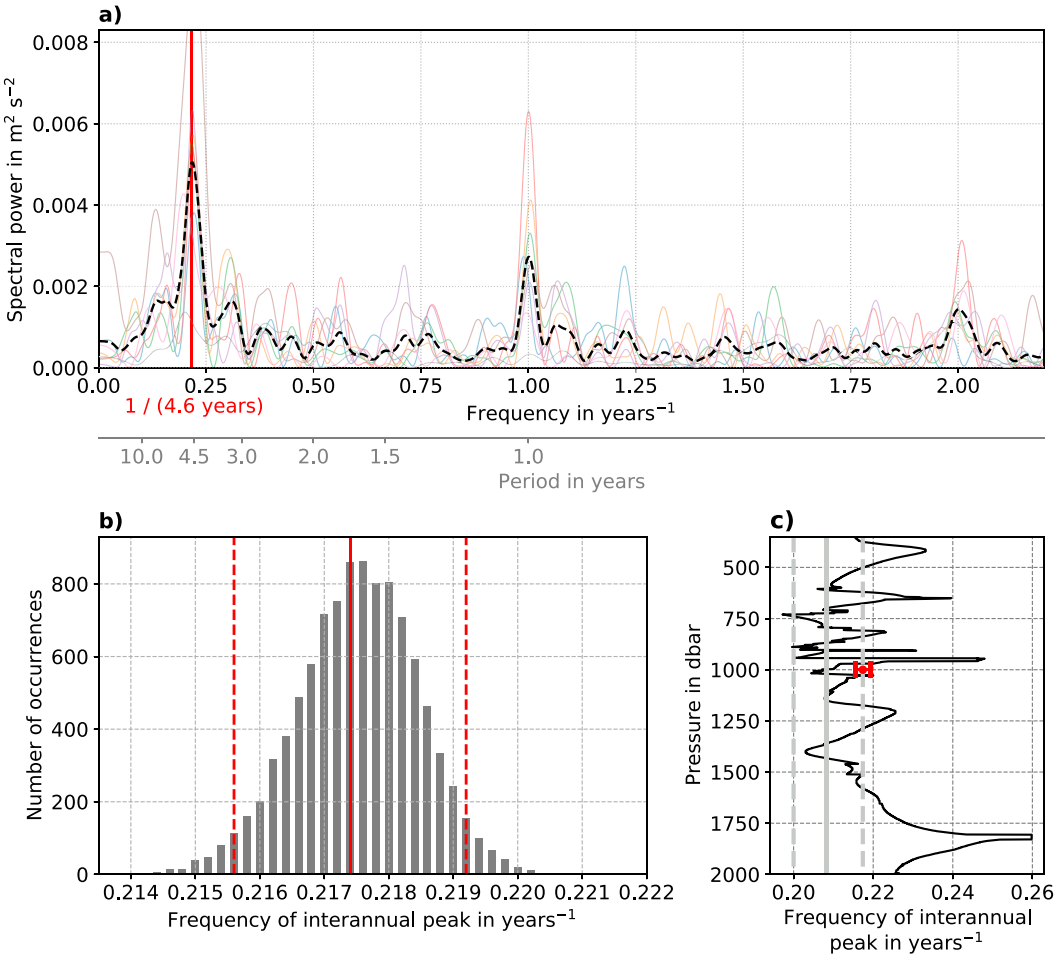

FIG. 5. Frequency of the Atlantic EDJ. (a) Lomb–Scargle periodograms of equatorial zonal velocity at 1000-m depth in the Atlantic Ocean, separated into bins from 1°S to 1°N and of 5° width in longitude (thin colored lines). The thick black dashed line is the average of all individual periodograms. (b) Distribution of interannual peak frequency of Atlantic Ocean equatorial zonal velocity at 1000-m depth as determined by bootstrapping. The solid red line indicates the value calculated from the original dataset, and the dashed lines mark the 2.5% and 97.5% quantiles of the distribution. (All parameter estimations and confidence intervals are summarized in Table 1.) (c) Comparison of YoMaHa-based estimate (red) with estimate from mooring data at 23°W (black) and the estimate from Youngs and Johnson (2015) (gray). The estimate by Youngs and Johnson (2015), averaged between 400 and 3000 dbar, is indicated by the gray solid line, and their 95% confidence interval is shown by the dashed gray lines.

much larger range of estimates from the mooring data, and just within the confidence interval from Youngs and Johnson (2015), which is shifted toward lower frequencies.

b. *Amplitude at 1000-m depth*

To estimate the shape that the EDJ assume in the basin, we calculate their amplitude at 1000-m depth on a 0.2° × 0.2° grid in the equatorial Atlantic basin. We do this by smoothing the zonal velocity field from the YoMaHa'07 dataset using the smoothing procedure described in section 2b(2), followed by least squares fitting of a cosine function of the form

$$u_{\text{fit}} = A\cos(\omega t + \varphi) \tag{9}$$

at every longitude and latitude on the 0.2° × 0.2° grid, where the amplitude A and the phase φ are free parameters to be fitted, t is the time (chosen such that $t = 0$ corresponds to 1 January 2000), and the angular frequency $\omega = 2\pi f_{\text{EDJ}}$ is fixed to the EDJ frequency with $f_{\text{EDJ}} = 0.2174\ \text{yr}^{-1}$ (see section 3a). The resulting harmonic amplitude field can be seen in Fig. 6a. It has to be noted that the use of the harmonic amplitude here is likely the reason for the discrepancy between our amplitude estimates and the somewhat larger values that many instantaneous measurements suggest. Hereinafter, we omit the word harmonic when discussing our amplitude estimation.

In general, the EDJ are strongest directly on the equator, and their amplitude decreases quickly with increasing distance from the equator. This is in accordance with their appearance as a basin mode of a high baroclinic mode: the constituting parts, equatorial Kelvin and Rossby waves, are both characterized by a zonal velocity maximum on the equator. In the

TABLE 1. Overview of the Atlantic EDJ characteristics. The boldface value in the center is always the value estimated from the original data. Values in parentheses above and below are the 0.025 and 0.975 quantiles of the parameter distribution obtained by bootstrapping. Frequency and zonal wavelength have been estimated for the entire basin instead of for the different 5° longitude bins. The period is not a parameter that has been separately estimated but rather is the reciprocal of the frequency, and it is included here for easier readability. The amplitude and phase have been estimated by a harmonic fit with the time origin at 1 Jan 2000. The vertical wavelength is given in stretched decibars. For a comparison with other estimates, the exact profile of N that we used for vertical stretching is necessary: this can be found in the supporting dataset (see the data availability statement for the link).

	40°–35°W	35°–30°W	30°–25°W	25°–20°W	20°–15°W	15°–10°W	10°–5°W	5°W–0°
				YoMaHa'07 (1000-m depth)				
Frequency (yr^{-1})				(0.2156) **0.2174** (0.2192)				
Period (years)				(4.64) **4.60** (4.56)				
Amplitude (cm s^{-1})	(6.0) **7.6** (9.3)	(7.6) **9.1** (10.7)	(8.4) **10.3** (12.2)	(9.1) **10.7** (12.4)	(8.5) **10.7** (12.9)	(8.3) **9.9** (11.6)	(3.3) **4.7** (6.3)	(2.4) **3.7** (5.1)
Phase	(0.109) **0.285** (0.454)	(0.190) **0.374** (0.608)	(0.433) **0.567** (0.722)	(0.555) **0.727** (0.894)	(0.705) **0.833** (0.960)	(0.824) **0.984** (1.152)	(1.319) **1.583** (1.920)	(1.494) **1.797** (2.046)
Zonal wavelength (°)				(126.3) **146.7** (177.4)				
				Hydrographic Argo data (400–2000-m depth)				
Vertical wavelength (sdbar)	(621) **592** (457)	(498) **474** (457)	(505) **488** (474)	(500) **488** (476)	(571) **524** (465)	(500) **493** (463)	(510) **498** (485)	(595) **549** (463)

center of the basin (and a bit to the west), the EDJ are narrowest and strongest; toward the east and west they become broader and eventually seem to split into two off-equatorial maxima. This is reminiscent of the zonal velocity amplitude fields of modeled basin modes shown in Greatbatch et al. (2012) and Claus et al. (2014), where β dispersion leads to focusing of long off-equatorial Rossby waves in the center of the basin (Schopf et al. 1981) and thus a narrowing of the basin mode amplitude field. Claus et al. (2014) suggest that this focusing effect is suppressed by the barotropic mean flow around the equator. However, the midbasin narrowing of the EDJ amplitude field estimated here indicates that the equator is not entirely shielded by the barotropic mean flow, but that some focusing of energy in the center of the basin does take place.

To estimate the uncertainty of the EDJ amplitude on the equator, we again apply bootstrapping, and we use the original unsmoothed data. Because the amplitude of the EDJ clearly depends on longitude, we separate the YoMaHa'07 zonal velocity data into 5° wide bins, and estimate the amplitude for each of these individually by fitting a sine wave with the frequency that we estimated in section 3a (0.2174 yr^{-1}). Because the amplitude of the EDJ is quite sensitive to the distance to the equator, as is visible in Fig. 6a, we restricted the bins to 0.5°S to 0.5°N for this calculation. The resulting EDJ amplitude values, together with the 95% confidence intervals, can be seen in Fig. 6b and Table 1. Between 25° and 15°W, the amplitude is largest, reaching almost 11 cm s^{-1}. Toward the west and east, it decreases, reaching 7.6 cm s^{-1} between 40° and 35°W and only 3.7 cm s^{-1} between 5°W and 0°E.

In Fig. 6c, the EDJ amplitude estimated from the 23°W mooring dataset is shown for comparison. Around 1000-m depth, the data coverage from the mooring is sparse (cf. Fig. 2), such that the amplitude estimation is relatively noisy. However, it agrees well with the estimate from the YoMaHa'07 data. The strong modulation of the EDJ amplitude with depth that is visible in the mooring data may be explained by the superposition of the vertical structures of the normal modes of which the EDJ are dominantly composed (Claus et al. 2016).

c. *Phase and zonal wavelength at 1000-m depth*

We calculate the phase of the EDJ harmonic in the equatorial Atlantic by a least squares fit of Eq. (9) to the smoothed zonal velocity field at 1000-m depth as described in section 3b.

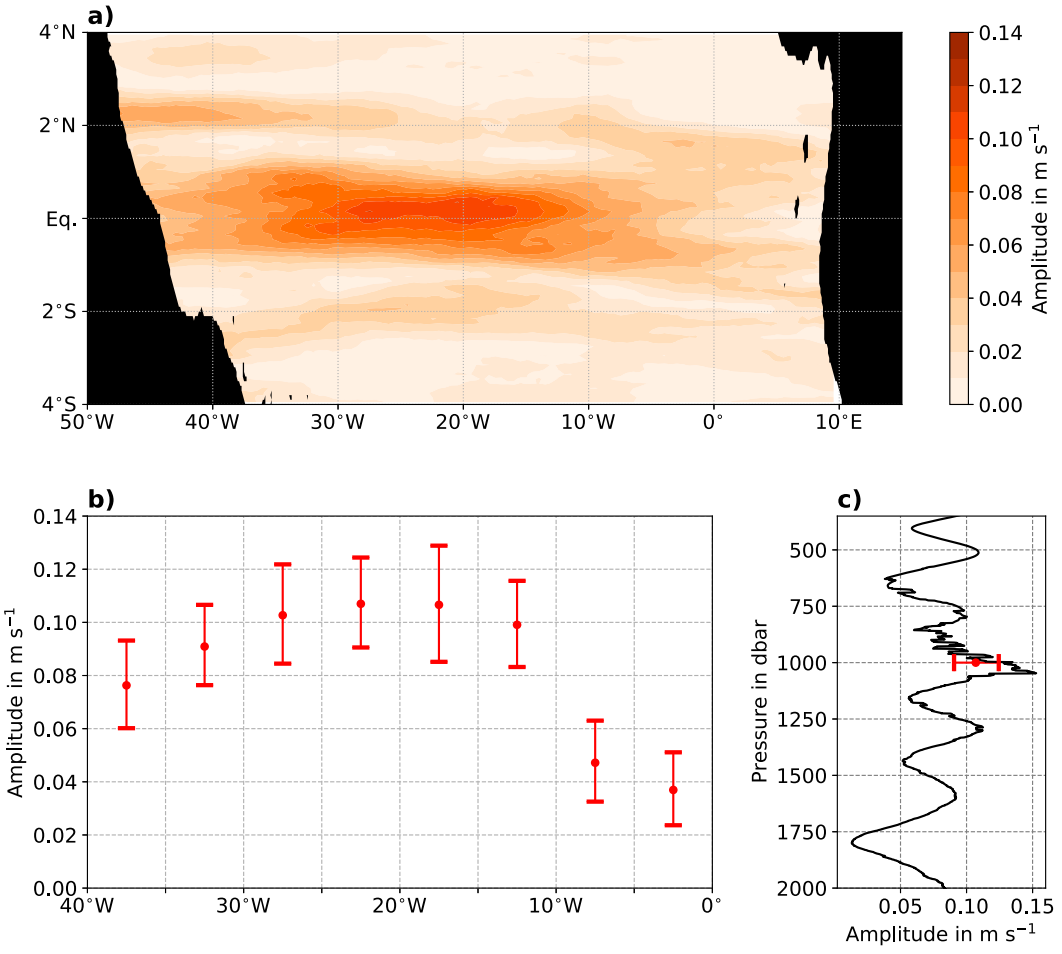

FIG. 6. Harmonic amplitude of the Atlantic equatorial deep jets. (a) The amplitude of a harmonic fit at the estimated EDJ frequency of 0.2174 yr^{-1} to the smoothed zonal velocity field from YoMaHa'07 [for details on the smoothing see section 2b(2)]. (b) EDJ amplitude values along the equator, estimated from the original, unsmoothed data between 0.5°S and 0.5°N and from 5° longitude bins. The error bars mark the 2.5% and 97.5% quantiles of the distribution obtained by bootstrapping (these values can also be found in Table 1). (c) A comparison with mooring data from 23°W. The harmonic EDJ amplitude from the mooring data is shown in black, with the corresponding value and confidence interval from the YoMaHa'07 dataset (from 25° to 20°W) in red for comparison.

In Fig. 7a, the EDJ phase estimated from the smoothed zonal velocity field at 1000-m depth is shown. The phase field is characterized by zonal bands with mostly westward phase propagation and sudden phase shifts by π between them, which shows the signature of long equatorial Rossby waves. In Fig. 7b and Table 1, the EDJ phase on the equator is shown, together with the 95% confidence intervals from bootstrapping. For comparison, the EDJ phase values estimated from the 23°W mooring data are shown in Fig. 7c, and they fit nicely to the estimate from the YoMaHa'07 data.

We can obtain the zonal propagation direction and wavelength by evaluating the change of EDJ phase with longitude. The zonal derivative of the EDJ phase is shown locally for every grid point in Fig. 8a. Although the field is noisy, the EDJs' westward phase propagation on the equator is clearly visible. North and south of the equator, bands of eastward phase propagation appear where the equatorial Kelvin wave dominates the signal.

We calculate the Atlantic EDJs' mean basinwide zonal wavelength by linear regression, that is, fitting a straight line to the phase–longitude relationship shown in Fig. 7b. The zonal wavelength λ_z can then be obtained from the regression slope (zonal wavenumber) k as

$$\lambda_z = 2\pi/k. \tag{10}$$

The result can be seen in Fig. 8b. On the equator, the zonal wavelength of the Atlantic EDJ is 146.7° (indicated by the red marker; 95% confidence interval between 126.3° and 177.4°), which is between the wavelength of an equatorial Kelvin wave and that of a first meridional mode Rossby wave with the corresponding frequency and vertical mode of the EDJ (see Fig. 8b). As visible in Fig. 8b, the zonal wavelength of the variability at the EDJ frequency is very much dependent on latitude, because of the differences in the meridional structure

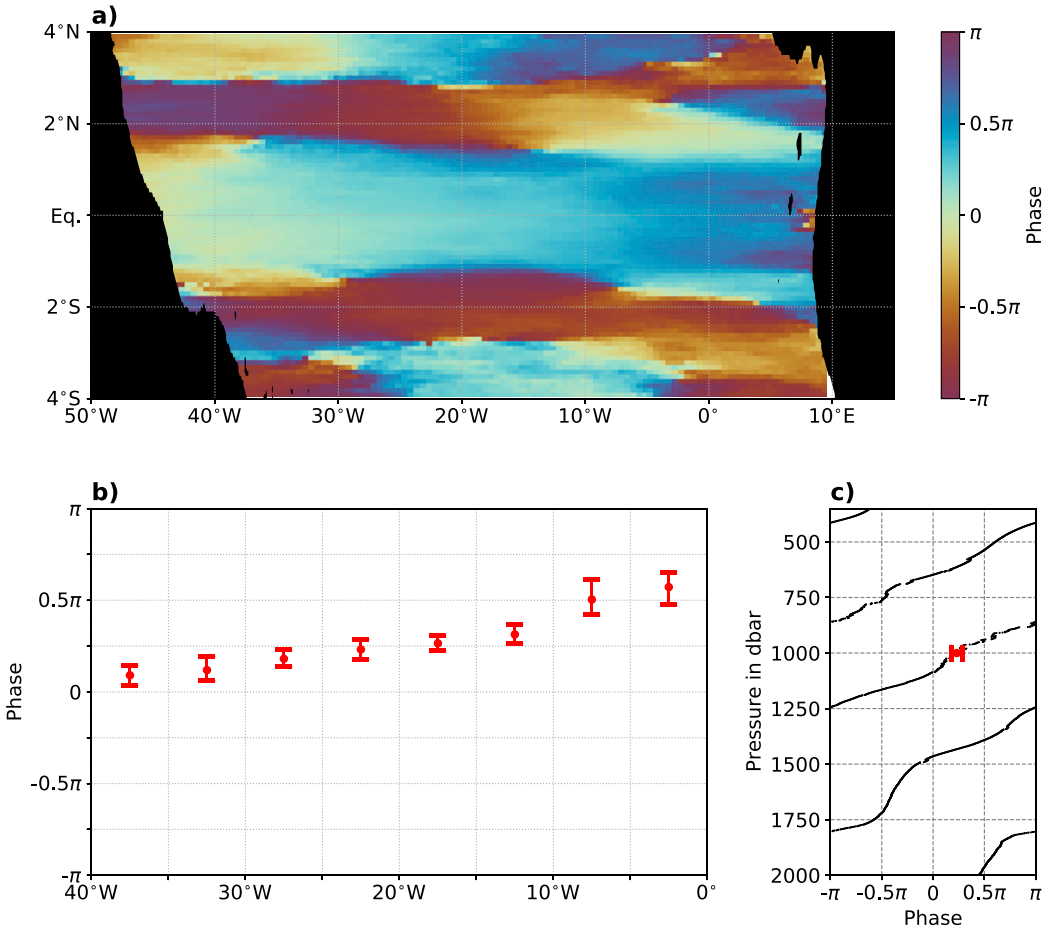

FIG. 7. Phase of the Atlantic EDJ. The phase values φ are calculated by a least squares fit of a cosine function of the form $A\cos(\omega t + \varphi)$ to the YoMaHa'07 zonal velocity data. The time axis t for the fit has been chosen such that the origin ($t = 0$) is 1 Jan 2000. The angular frequency $\omega = 2\pi \times 0.2174\ \mathrm{yr}^{-1}$ has been fixed to the estimated EDJ frequency value. (a) Phase estimated from the smoothed zonal velocity field. (b) Phase values along the equator calculated from the original, unsmoothed data (from between 1°S and 1°N and separated into 5° longitude bins). The error bars mark the 2.5% and 97.5% quantiles obtained by bootstrapping (for all of these values see also Table 1). (c) Comparison with mooring data from 23°W. The EDJ phase from the mooring data is shown in black, with the corresponding value and confidence interval from the YoMaHa'07 dataset (from 25° to 20°W) in red for comparison.

of the Kelvin and Rossby waves that together constitute the EDJ. North of the equator, the zonal wavelength of the EDJ first increases, getting closer to the Kelvin wavelength, and then decreases to approximately the wavelength of the Rossby wave. South of the equator, the pattern is not as clear. Our estimates are consistent with the model results from Claus et al. (2016, see their Fig. 7a), and also with Youngs and Johnson (2015), who only estimated the zonal wavelength of the Rossby wave component of the Atlantic EDJ based on vertical strain at 1.5°S/N.

d. *Meridional structure at 1000-m depth and contributions of Kelvin and Rossby wave signals*

It has been noted by a number of earlier studies that the EDJ show characteristics of an equatorial basin mode (e.g., d'Orgeville et al. 2007; Greatbatch et al. 2012; Ascani et al. 2015; Matthießen et al. 2015, 2017). Equatorial basin modes consist of the resonant combination of an equatorial Kelvin wave and its reflection as a sum of odd meridional mode long equatorial Rossby waves (Cane and Moore 1981). To find out how large the contributions of the different equatorial waves are to the total EDJ amplitude, we separate the zonal velocity data from 1000-m depth into a Kelvin wave component and a Rossby wave component.

The meridional structure of the zonal velocity signature is given by (cf. Gill 1982, chapter 11)

$$u_K(y) = u_{0\_K} \exp\left(-\frac{\beta y^2}{2c}\right) \tag{11}$$

for an equatorial Kelvin wave and by

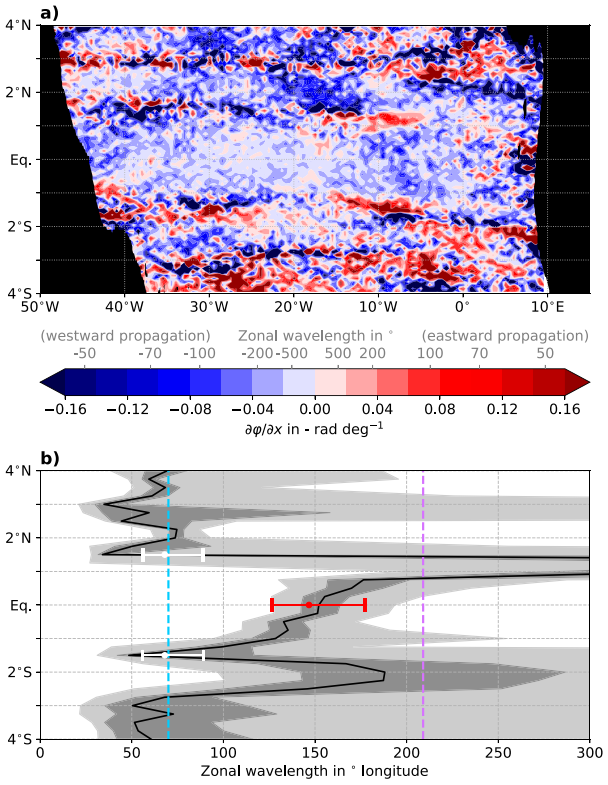

FIG. 8. Zonal wavelength of the Atlantic EDJ at 1000-m depth. (a) The change of EDJ phase (as shown in Fig. 7a) with longitude, i.e., $\partial\varphi/\partial x$, and the associated zonal wavelength. Blue shading means westward propagation of the EDJ harmonic, and red colors indicate eastward propagation. (b) The absolute value of the zonal wavelength estimated by linear regression of the EDJ phase between 40°W and 0°E. Indicated in red is the estimate and 95% confidence interval from the original data between 1°S and 1°N. To examine the change with latitude, the zonal EDJ wavelength is shown for different latitudes in black, but now with only 1° wide latitude bins to show more detail. The dark-gray shading indicates the 50% confidence interval, and the light-gray shading indicates the 95% confidence interval. In white, the estimate and 95% confidence interval from Youngs and Johnson (2015) are shown. The theoretical Kelvin wavelength is shown by the dashed purple line, and the meridional mode-1 Rossby wavelength is shown by the dashed blue line, both for a frequency of $f_{EDJ} = 0.2174$ yr^{-1} and a gravity wave speed of $c = 0.16$ m s^{-1} corresponding to vertical mode 17.

$$u_{Rn}(y) = u_{0\_R_n} \exp\left(-\frac{\beta y^2}{2c}\right) \times \left[\left(c - \frac{c}{2n+1}\right) 2^{-(n+1)/2} H_{n+1}\left(\sqrt{\frac{\beta}{c}}y\right) - \left(c + \frac{c}{2n+1}\right) n 2^{-(n-1)/2} H_{n-1}\left(\sqrt{\frac{\beta}{c}}y\right)\right] \quad (12)$$

for long equatorial Rossby waves with meridional mode number n. The u_{0_K} and $u_{0\_R_n}$ denote constant amplitude values, y is the distance from the equator measured positive northward, $\beta = 2.3 \times 10^{-11}$ m^{-1} s^{-1} (Gill 1982, chapter 11) is the change of the Coriolis parameter with latitude, and H_n denotes the nth Hermite polynomial. The dominant vertical mode 17 and corresponding gravity wave speed $c = 0.16$ m s^{-1} of the EDJ have been estimated by a normal mode decomposition of the moored zonal velocity measurements from 23°W, using a mean stratification profile from the surface to 4500-m depth obtained from equatorial cruise data, as described in detail in Claus et al. (2016). The stratification profile calculated from Argo float data (Fig. 4) only extends to 2000-m depth, such that it cannot be used for the normal mode decomposition. However, in the upper 2000 m it is similar to the mean stratification profile obtained from the cruise data (not shown), such that no large changes to the estimated gravity wave speed of the EDJs' dominant vertical mode would be expected when using different data.

The meridional structure of the Atlantic EDJ amplitude field shown in Fig. 6a is strongly reminiscent of the zonal velocity amplitude structure of a first meridional mode Rossby wave, with the equatorial maximum, followed by a minimum and a second maximum with increasing distance from the equator. However, the distance from the equator of the off-equatorial amplitude minima of the EDJ in Fig. 6a is larger by a factor of 1.5 than expected from inviscid theory for the particular choice of c from Eq. (12), even in the center of the basin (around 20°W) where the EDJ are narrowest. This is consistent with the general agreement in different earlier studies that investigated the meridional width of the EDJ and found that the observed EDJ are widened by a factor of 1.5 in the meridional direction relative to inviscid theory (e.g., Johnson and Zhang 2003; Greatbatch et al. 2012; Claus et al. 2014; Youngs and Johnson 2015). A physical explanation for the enhanced meridional width of the EDJ relative to inviscid theory was provided by Greatbatch et al. (2012), who attributed it to relatively large dissipation of momentum in combination with relatively weak diapycnal mixing in the deep equatorial ocean. Greatbatch et al. (2012) argue that the zonal flow along the equator is to a good approximation in geostrophic balance for a baroclinic equatorial basin mode. Reducing the strength of this flow by large momentum dissipation requires, by thermal wind, a reduced meridional density gradient north and south of the equator. If the diapycnal mixing is too weak to remove the equatorial density perturbation supporting the flow, the meridional width of the flow must then be larger than given by inviscid theory. However, the exact contributions of different processes on the meridional widening of the EDJ are still a topic for further research. To investigate the causes of the widening is beyond the scope of this article; but for the fitting of the meridional amplitude structure of the EDJ we of course have to account for this well known EDJ characteristic. We therefore stretched the theoretical inviscid profiles given by Eqs. (11) and (12) meridionally by a factor of 1.5 before fitting them to the estimated EDJ amplitude profile, thereby empirically accounting for the effect of viscous processes not included in the inviscid Eqs. (11) and (12).

We determined the amplitude and phase of the EDJs' Kelvin wave component by doing a harmonic fit at the EDJ frequency to the zonal velocity field. The amplitude and phase

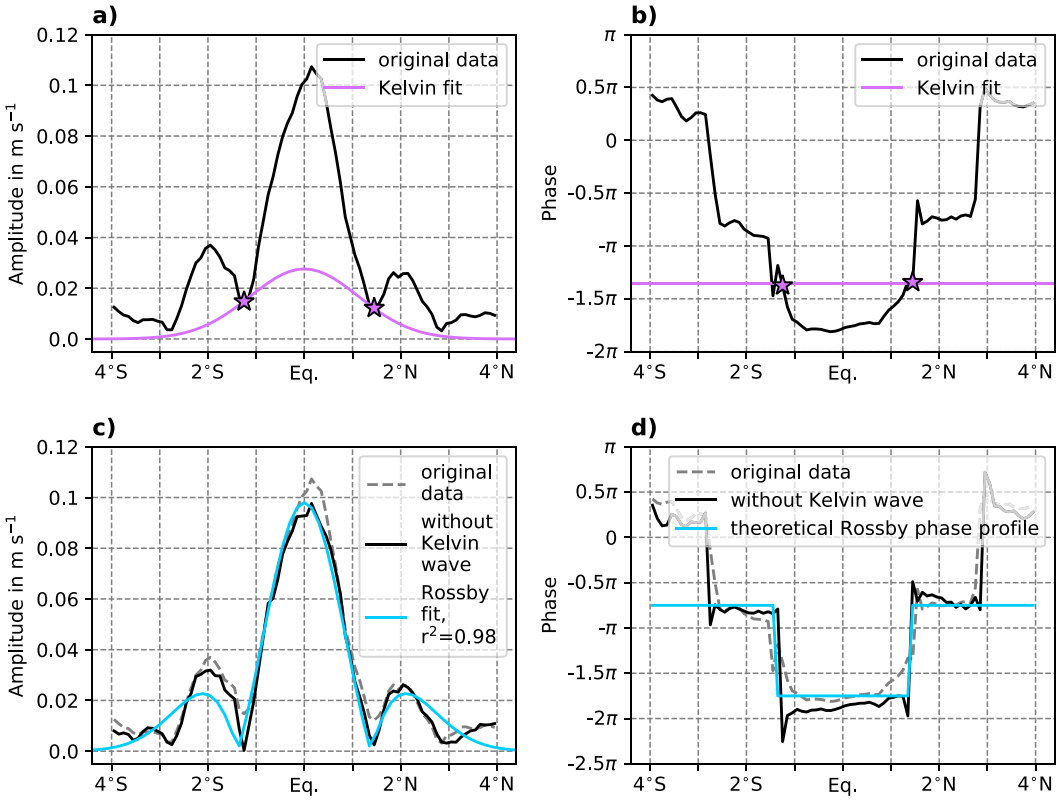

FIG. 9. Amplitude and phase of the Kelvin and first meridional mode Rossby wave components of the Atlantic EDJ at 1000-m depth, averaged between 28° and 17°W where the EDJ are strongest. The meridional profiles of EDJ (a) amplitude and (b) phase are shown in black. The purple stars indicate the values used to reconstruct the Kelvin wave profiles (shown as purple lines). Also shown are the (c) amplitude and (d) phase profiles after removing the Kelvin wave signal, in black (for comparison, the original data are shown in gray). The fit of a first meridional mode Rossby wave to the remaining data is shown in blue. Note that the theoretical Kelvin and Rossby wave profiles have been stretched meridionally by a factor of 1.5 (for details, see the text).

resulting from such a harmonic fit to the zonal velocity, averaged between 28° and 17°W where the EDJ are strongest, are shown in Figs. 9a and 9b in black. At the latitudes where the zonal velocity signature of the Rossby wave has zero amplitude (at approximately 1.35°S/N when stretched by a factor of 1.5), the Kelvin wave signal should dominate the EDJs' zonal velocity field. Marked with a purple star are the amplitude (Fig. 9a) and phase (Fig. 9b) values at the minima of the amplitude profile shown in black in Fig. 9a, located a little asymmetrically about the equator at approximately 1.25°S and 1.45°N, that we attribute to the Kelvin wave. The associated meridional profiles of the Kelvin wave amplitude and phase are drawn as purple lines. The equatorial amplitude maximum of the Kelvin wave is at a value of 2.8 cm s^{-1}.

With the amplitude and phase information, we can reconstruct a Kelvin wave signal that oscillates in time at the EDJ frequency. This is substracted from the time-varying zonal velocity between 28° and 17°W. A new harmonic fit at the EDJ frequency is then performed with the residual velocity field; the resulting amplitude and phase are shown in Figs. 9c and 9d. Fitting of the theoretical amplitude [Eq. (12)] and phase profiles of a first meridional mode Rossby wave to these data then yields the results shown in blue in Figs. 9c and 9d. The equatorial amplitude maximum of the first meridional mode Rossby wave is with 9.8 cm s^{-1} much larger than that of the Kelvin wave component.

Poleward of about 2.5°S/N, the influence of higher-mode Rossby waves is visible in the repeated amplitude minimum and π phase shift that cannot be accounted for by the fit shown in blue in Figs. 9c and 9d. Shown in Fig. 9 are only results using data from the center of the basin, where the EDJ signal is strongest—repeating the analysis with data from farther east yielded less significant results because of larger contributions from higher-mode Rossby waves (not shown).

e. *Vertical structure on the equator*

We used the hydrographic data that are measured by the Argo floats during descent/ascent to reconstruct the geostrophic zonal velocity at depth, using the YoMaHa'07 data at 1000-m depth as reference [see section 2b(4)].

In Fig. 10, a comparison of the reconstructed geostrophic velocity from hydrographic Argo data between 20° and 25°W with the velocity measured by moored current meters at 23°W is shown. The reconstructed zonal velocity (Fig. 10b) was

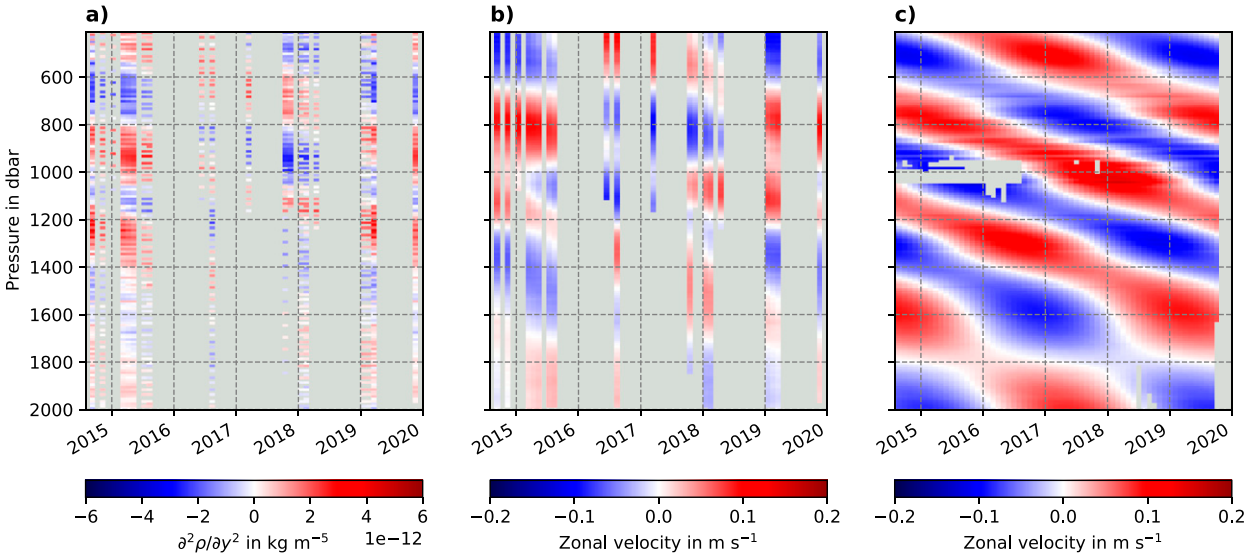

FIG. 10. Reconstructed equatorial geostrophic zonal velocity from hydrographic Argo float data between 25° and 20°W. (a) Second meridional derivative of in situ density, calculated from Argo float temperature and salinity measurements, averaged monthly and between 25° and 20°W. Because the data were otherwise too noisy, they have been temporally filtered by performing a harmonic fit at the EDJ frequency and removing all other variability. (b) Geostrophic zonal velocity as calculated using Eq. (6) from the data shown in (a), referenced with (harmonically filtered in time) Argo float displacement data from YoMaHa'07 at 1000-m depth and detrended vertically (for details, see the text). (c) Moored equatorial zonal velocity measurements at 23°W for comparison (also harmonically filtered in time).

originally dominated by strong, but apparently random, linear vertical trends. We suspect that these are spurious and due to the vertical integration of systematic errors in the original Argo float measurements, possibly caused by drift of the salinity sensors. Associated depth-independent salinity errors might lead to small depth-independent offsets in the density of some profiles, which, when vertically integrated, results in a linear trend in the velocity profile. These trends have been removed before further analysis; shown in Fig. 10 is the vertically detrended zonal velocity. The data have additionally been temporally filtered to remove noise on other time scales than the EDJ frequency. The reconstructed geostrophic zonal velocity generally compares well to the zonal velocity measurements from the 23°W mooring, and seems to capture the EDJ very well. Some disagreements are visible, however. Several reasons could contribute to these differences—for example, ageostrophic velocities that are included in the mooring data but not in the reconstructed velocity from Argo, as well as sparse data coverage from the Argo float hydrographic data (the bins used to calculate the second meridional derivative of density often contain a single profile only).

To estimate the vertical wavelength of the Atlantic EDJ, we again make use of the Lomb–Scargle periodogram to calculate vertical wavenumber spectra of the zonal velocity. We choose wavenumbers with a resolution of 1×10^{-5} sdbar^{-1}, which corresponds to a wavelength resolution of approximately 2.5 sdbar around 500 sdbar (here "sdbar" indicates "stretched decibars"). In Fig. 11, the resulting spectra are shown from the reconstructed zonal velocity from Argo from between 20° and 25°W (Fig. 11a) and, for comparison, from the 23°W moored velocity measurements (Fig. 11b). Note that the data have been stretched and scaled before spectral analysis to remove the influence of variable stratification with depth [for details see section 2b(5)], as well as temporally filtered to get rid of noise on time scales different from that of the EDJ. In Fig. 11c, the peak vertical wavelength is shown for all longitudes, together with a 95% confidence interval obtained by bootstrapping. The value and confidence interval from the mooring data are drawn in black, and it can be seen that, although the difference between the estimated vertical EDJ wavelengths is only about 20 sdbar (with 488 sdbar from the Argo data between 25° and 20°W, and 467 sdbar from the mooring data at 23°W), the confidence intervals do not overlap. This seemingly significant difference, as well as the very small confidence interval of the mooring data, indicates deficiencies in our error estimation—it seems that, in this case, there is an additional source of error beside the sampling uncertainty that cannot be quantified by bootstrapping. The basinwide estimate by Youngs and Johnson (2015) from shipboard CTD measurements, which is shown in gray, compares well to our estimates.

4. Discussion

a. *A new characterization of the Atlantic EDJ*

In this study, we have compiled a new, independent, more comprehensive and accurate description of the Atlantic equatorial deep jets (EDJ) than available so far. For this, we have analyzed Argo float displacement data at 1000-m depth (Lebedev et al. 2007) and Argo float hydrographic profiles (Argo 2020). At 1000-m depth, we provide estimates of the

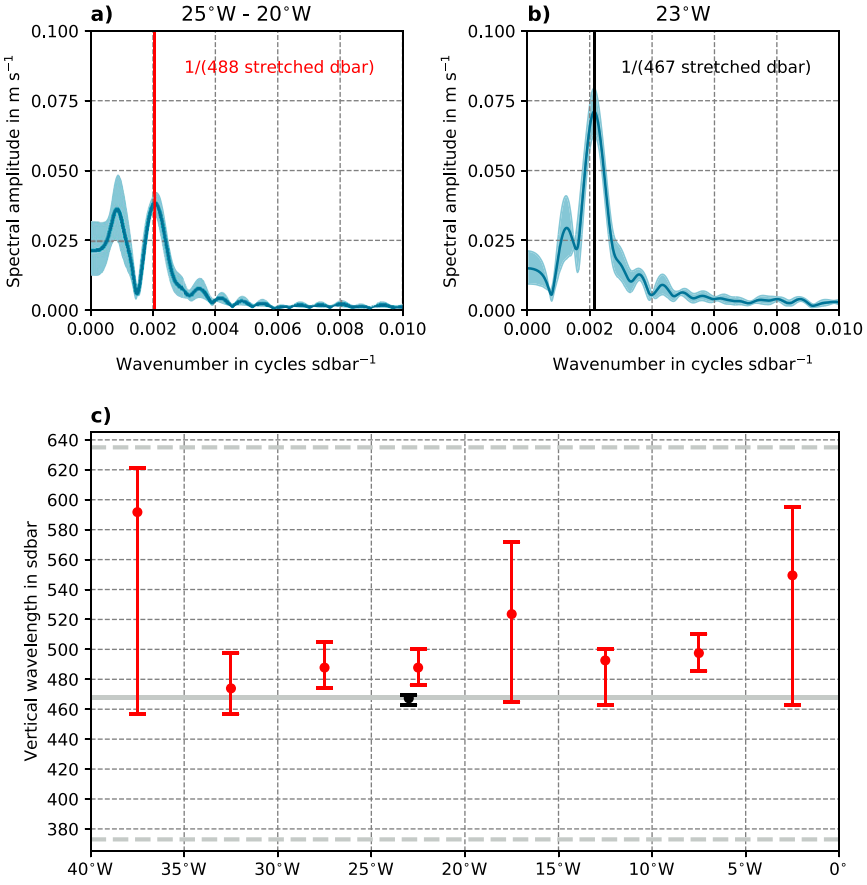

FIG. 11. Vertical wavelength of the Atlantic EDJ on the equator. (a) Vertical wavenumber spectrum of (stretched and scaled) equatorial geostrophic zonal velocity between 400- and 2000-m depth and between 20° and 25°W, reconstructed from hydrographic Argo float data. Because the data were otherwise too noisy, they were temporally filtered to contain only variability on the EDJ frequency. The solid blue line indicates the mean of all spectra calculated separately for each monthly profile, and the area between the 25% and the 75% quantile of all spectra is shaded. The location of the EDJ peak is indicated in red, with corresponding red text. (b) As in (a), but from equatorial zonal velocity at 23°W measured by moored current meters for comparison. Here the EDJ peak is indicated in black. (c) Location of EDJ peak with 95% confidence intervals for all 5° longitude, 1°S–1°N bins (in red). The value and confidence interval from the mooring data are drawn in black. For comparison, the vertical wavelength estimate by Youngs and Johnson (2015) from shipboard CTD measurements is indicated by the solid gray line, and their 95% confidence interval is shown by the thick dashed gray lines.

period, the amplitude, the phase, the zonal wavelength, and the meridional structure of the Atlantic EDJ. Our EDJ period estimate of 4.60 yr (95% confidence interval between 4.56 and 4.64 yr) fits well to earlier estimates using the moored velocity measurements from 23°W (e.g., Brandt et al. 2011; Claus et al. 2016; Greatbatch et al. 2018), and also confirms the most recent basinwide estimate from shipboard CTD measurements by Youngs and Johnson (2015), but with a smaller confidence interval. Our EDJ amplitude and phase estimates from the Argo float displacement data represent the first detailed assessment of the basinwide horizontal structure of the Atlantic EDJ, albeit only at 1000-m depth: the horizontal shape that the EDJ assume in the basin has so far only been assessed with models (e.g., Greatbatch et al. 2012; Claus et al. 2014, 2016). In our results it can be seen that the Atlantic EDJ are slightly narrower by about 0.1°–0.2° in the basin center than toward the west and east (Fig. 6a), which is suggestive of long Rossby wave focusing due to β dispersion (Schopf et al. 1981). This focusing effect is likely reduced by the mean flow around the equator, as well as by momentum dissipation (Claus et al. 2014; Greatbatch et al. 2012), but evidently not prevented completely. The zonal wavelength of the Atlantic EDJ is highly dependent on latitude, because of the

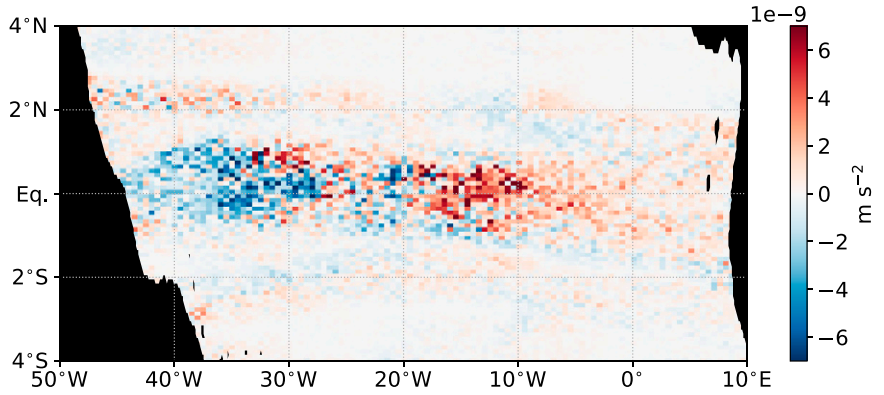

FIG. 12. Acceleration of the mean zonal currents at 1000-m depth through the zonal self-advection of the Atlantic EDJ (for details, see the text).

different meridional structures and zonal wavelengths of the constituting Kelvin and Rossby wave components (Fig. 8b). Our estimate confirms and complements the estimate of Youngs and Johnson (2015), who only calculated the zonal wavelength of the Rossby wave component, but not the zonal wavelength of the entire EDJ on the equator, which is at 147° (95% confidence interval between 126° and 177°) about twice as large as that of the Rossby wave component alone. Claus et al. (2016) have found similar results with a shallow water model of the Atlantic EDJ, with a zonal EDJ wavelength on the equator of approximately 150°.

Since the Argo float displacement data are only abundant at 1000-m depth, it is not possible to estimate the vertical scale of the EDJ. Instead, we estimate it from hydrographic profiles measured by the floats, using the fact that the EDJ are approximately in geostrophic balance. Our results compare well to the estimate from Youngs and Johnson (2015), and even have confidence intervals that are smaller by about 20%–80%, depending on the longitude (Fig. 11c). There is also no systematic change of vertical EDJ scale with longitude visible in our results.

Our results confirm the similarity of the Atlantic EDJ to a resonant equatorial basin mode (Cane and Moore 1981), which has been suggested by several modeling studies (e.g., d'Orgeville et al. 2007; Ascani et al. 2015; Matthießen et al. 2015, 2017) and from analysis of the EDJ period and vertical scale from the moored velocity measurements at 23°W (e.g., Claus et al. 2016; Greatbatch et al. 2018). The theoretical period for the gravest equatorial basin mode is given by

$$T_n = 4L/c_n, \tag{13}$$

where L is the width of the basin and n is the baroclinic mode number. If we take $L = 52°$ as the width of the equatorial Atlantic at 1000-m depth and $c_n = 0.16$ m s^{-1} for the dominant vertical mode of the EDJ $n = 17$, as determined by a vertical mode decomposition of the moored zonal velocity measurements from 23°W as described in detail in Claus et al. (2016), we get a theoretical EDJ period of $T_n = 4.57$ yr, which fits well to our estimate of 4.6 ± 0.04 yr. We also find that the amplitude of the Atlantic EDJ is largest in the central part of the basin (though not exactly in the basin center, see below), and decreases toward the western and eastern boundaries. Furthermore, the Atlantic EDJ signal that we find in Argo data is dominantly composed of an equatorial Kelvin wave and a first meridional mode Rossby wave, with some contribution from higher meridional mode Rossby waves close to the eastern boundary. All this corresponds well to the structure of a resonant equatorial basin mode (Cane and Moore 1981).

However, there are also some differences between the EDJ in the real Atlantic Ocean and a theoretical (linear) equatorial basin mode as described by Cane and Moore (1981). In the latter, the amplitudes of the equatorial Kelvin wave and the first meridional mode Rossby wave should be similar (Cane and Moore 1981; Cane and Sarachik 1977), but our results confirm the finding of Youngs and Johnson (2015) that the Atlantic EDJ are dominated by a Rossby wave signal with much larger amplitude in comparison with the Kelvin wave signal. This seems to be a special feature of the Atlantic EDJ, since Youngs and Johnson (2015) find that in the Indian and Pacific Oceans the equatorial Kelvin and first meridional mode Rossby wave have approximately the same amplitude. A possible explanation could be topographic differences between the oceans, for example, the distinctive Gulf of Guinea in the Atlantic, that might lead to an asymmetry in the energy of the EDJ wave components. Another difference between the real Atlantic EDJ and a theoretical equatorial basin mode is the location of the zonal velocity amplitude maximum. Theoretical linear basin modes have their zonal velocity maximum in the center of the basin (Cane and Moore 1981), whereas our Argo data analysis shows that the amplitude maximum of the Atlantic EDJ is not located in the basin center but shifted to the west by about 5° (Fig. 6a). Also, the phase difference between the Kelvin and the first meridional mode Rossby wave in the center of the basin is approximately 1.4π, although it should be π for a theoretical basin mode. These differences could be indications of the effect of nonlinearity on the appearance of equatorial basin modes in the real ocean.

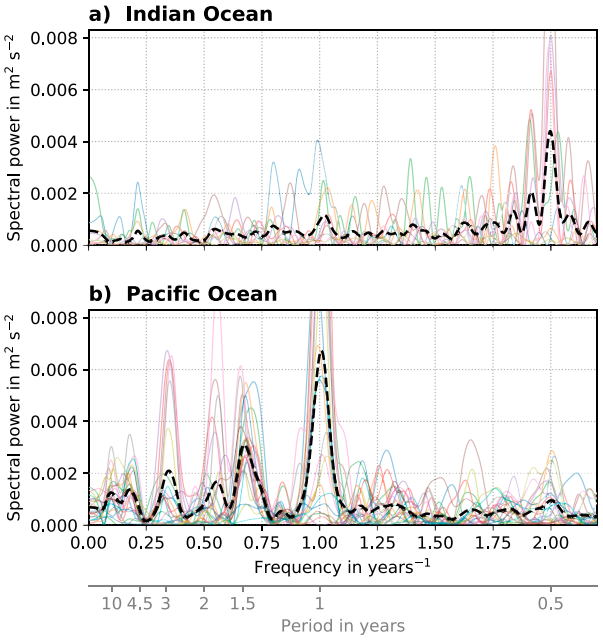

FIG. 13. Lomb–Scargle periodograms of zonal velocity at 1000-m depth along the equator in the (a) Indian and (b) Pacific Oceans, from the YoMaHa'07 dataset. The zonal velocity has been separated into bins from 1°S to 1°N and of 5° width in longitude (thin colored lines). The thick black dashed line is the average of all individual periodograms.

b. *Nonlinear acceleration of time-mean zonal flow by Atlantic EDJ*

It has been suggested by idealized model studies that the EDJ nonlinearly transfer some energy to the time-mean zonal currents at depth (Ascani et al. 2015; Bastin et al. 2020). The term that has been found to be largely responsible for this energy transfer in the models is the zonal self-advection of the EDJ, or

$$-\frac{\partial(\overline{u'u'})}{\partial x}, \tag{14}$$

where the overbar denotes a time average and u' is the zonal velocity variability at a time scale of 4.6 yr, that is, the Atlantic EDJ. We calculate this term from the Argo observations of the Atlantic EDJ at 1000-m depth, to see whether this can confirm the model results. The acceleration of the mean zonal flow due to (14) is shown in Fig. 12. Indeed, the acceleration due to the zonal self-advection of the EDJ in the Argo data shows very similar patterns as suggested by the model studies. In the western part of the basin, the EDJ strengthen the equatorial mean westward flow, as well as the flanking mean eastward jet at about 2°N (although for the flanking jet, the acceleration is weak relative to that at the equator, and for the corresponding eastward jet at 2°S the signal is not clear, suggesting a slight southward shift rather than a positive acceleration). In the center of the basin, however, where the EDJ have their amplitude maximum, the sign of their zonal self-advection changes, leading to eastward acceleration of the mean zonal flow on the equator in the eastern part of the basin. Bastin et al. (2020) argue that this eastward acceleration by the EDJ leads to a reversal of the originally westward time-mean zonal flow on the equator in the central and eastern basin, which potentially contributes to the ventilation of the eastern oxygen minimum zone.

c. *EDJ signals in the Indian and Pacific Oceans*

Previous studies have shown that in the Pacific and Indian Oceans, the EDJ signals have a smaller amplitude and are less coherent than in the Atlantic (e.g., Youngs and Johnson 2015). This is also visible in the Argo velocity data from 1000-m depth. In Fig. 13, Lomb–Scargle periodograms of zonal velocity at the equator are shown for the Indian and Pacific Oceans (the velocity values have been averaged between 1°S and 1°N, as well as over 5° longitude bins). In the Indian Ocean, the semiannual cycle stands out as the dominant peak in the spectrum. A very small peak is visible in the frequency range in which we would expect the Indian Ocean EDJ; at a frequency of about 0.22 yr^{-1}, but only at very few longitudes. These are located in the western part of the basin. The most dominant signal in the Pacific is the annual cycle, which has already been shown by Delpech et al. (2020a). No peak stands out at very low frequencies below 0.1 yr^{-1}, where the Pacific EDJ would appear. A possible reason for the absence of a Pacific EDJ signal in the Argo float displacement data at 1000-m depth is the long periodicity of the Pacific EDJ, which is estimated to be between 12 yr (Youngs and Johnson 2015) and several decades (Johnson et al. 2002), whereas there is sufficient data coverage in the YoMaHa'07 data only for the last 10 years. In the Indian Ocean, the absence of an EDJ signal could be due to the shallower midocean bathymetry, reaching up to about 1000 m. Measurements of the EDJ in the Indian Ocean have generally been made at shallower depths (e.g., Luyten and Swallow 1976). We thus suggest that more data or maybe data at different depths are needed to pick up the EDJ signals in the Indian and Pacific Oceans.

d. *Outlook*

An application for which this new estimation of Atlantic EDJ characteristics from Argo data might be highly relevant is the modeling of the tropical Atlantic Ocean. Despite the EDJs' likely importance for both interannual surface climate variability and deep ocean nutrient and oxygen transport, current ocean models and coupled forecasting systems are generally not able to faithfully simulate them. A possible way to include EDJ in ocean models or forecasting systems would be to add a forcing term to the momentum equation to create and maintain the currents, conceptually based on the real-world mechanism of momentum being fluxed into the EDJ due to the deformation of intraseasonal waves (Greatbatch et al. 2018; Bastin et al. 2020). For this, a forcing dataset is necessary that recreates the EDJs' characteristics as well as possible, and in particular the EDJs' phase needs to be estimated from a continuously running observing system like Argo or long-term current meter moorings.

Acknowledgments. The Argo float data were collected and made freely available by the international Argo project and

the national programs that contribute to it (see http://doi.org/10.17882/42182). Moored velocity data were acquired in cooperation with the PIRATA project. This study was funded in part by EU H2020 under Grant Agreement 817578 TRIATLAS project, by the Deutsche Forschungsgemeinschaft as part of the Sonderforschungsbereich 754 "Climate-Biogeochemistry Interactions in the Tropical Ocean" and through several research cruises with RV *Meteor* and RV *Maria S. Merian*, and by the German Federal Ministry of Education and Research (BMBF) as part of the projects NORDATLANTIK (03F0443B) and RACE-Synthese (03F0824C). All data analysis for this article has been done with Python. For visualization, we used Matplotlib (Hunter 2007), and Scientific Colour Maps 7 (Crameri 2018). The authors are not aware of financial conflicts/conflicts of interest related to this work. We thank Franz Philip Tuchen for updating and providing the moored velocity data from 0°N, 23°W. We are grateful to two anonymous reviewers for their helpful comments.

Data availability statement. The Argo float data are openly available through http://apdrc.soest.hawaii.edu/projects/Argo/data/trjctry/yomaha07.dat.gz (YoMaHa'07 deep velocity dataset; our version downloaded on 1 July 2020) and ftp://ftp.ifremer.fr/ifremer/argo/geo/atlantic_ocean/ (hydrographic Argo float profiles; our version downloaded on 20 July 2020). The mooring data can be accessed through www.pangaea.de or https://zenodo.org/record/4478285#.YNYNxC0es0o. All analysis scripts and supporting data have been published on Zenodo (doi.org/10.5281/zenodo.6327469).

REFERENCES

Argo, 2020: Argo float data and metadata from Global Data Assembly Centre (Argo GDAC). SEANOE, accessed 20 July 2020, https://doi.org/10.17882/42182.

Argo Data Management Team, 2019: Argo user's manual V3.3. Argo Doc., 111 pp., https://doi.org/10.13155/29825.

Ascani, F., E. Firing, P. Dutrieux, J. P. McCreary, and A. Ishida, 2010: Deep equatorial ocean circulation induced by a forced-dissipated Yanai beam. *J. Phys. Oceanogr.*, **40**, 1118–1142, https://doi.org/10.1175/2010JPO4356.1.

——, ——, J. P. McCreary, P. Brandt, and R. J. Greatbatch, 2015: The deep equatorial ocean circulation in wind-forced numerical solutions. *J. Phys. Oceanogr.*, **45**, 1709–1734, https://doi.org/10.1175/JPO-D-14-0171.1.

Bastin, S., M. Claus, P. Brandt, and R. J. Greatbatch, 2020: Equatorial deep jets and their influence on the mean equatorial circulation in an idealized ocean model forced by intraseasonal momentum flux convergence. *Geophys. Res. Lett.*, **47**, e2020GL087808, https://doi.org/10.1029/2020GL087808.

Brandt, P., V. Hormann, B. Bourlès, J. Fischer, F. A. Schott, L. Stramma, and M. Dengler, 2008: Oxygen tongues and zonal currents in the equatorial Atlantic. *J. Geophys. Res.*, **113**, C04012, https://doi.org/10.1029/2007JC004435.

——, A. Funk, V. Hormann, M. Dengler, R. J. Greatbatch, and J. M. Toole, 2011: Interannual atmospheric variability forced by the deep equatorial Atlantic Ocean. *Nature*, **473**, 497–500, https://doi.org/10.1038/nature10013.

——, and Coauthors, 2012: Ventilation of the equatorial Atlantic by the equatorial deep jets. *J. Geophys. Res.*, **117**, C12015, https://doi.org/10.1029/2012JC008118.

——, and Coauthors, 2015: On the role of circulation and mixing in the ventilation of oxygen minimum zones with a focus on the eastern tropical North Atlantic. *Biogeosciences*, **12**, 489–512, https://doi.org/10.5194/bg-12-489-2015.

——, M. Claus, R. J. Greatbatch, R. Kopte, J. M. Toole, W. E. Johns, and C. W. Böning, 2016: Annual and semiannual cycle of equatorial Atlantic circulation associated with basin-mode resonance. *J. Phys. Oceanogr.*, **46**, 3011–3029, https://doi.org/10.1175/JPO-D-15-0248.1.

Bunge, L., C. Provost, J. M. Lilly, M. d'Orgeville, A. Kartavtseff, and J.-L. Melice, 2006: Variability of the horizontal velocity structure in the upper 1600 m of the water column on the equator at 10°W. *J. Phys. Oceanogr.*, **36**, 1287–1304, https://doi.org/10.1175/JPO2908.1.

——, ——, B. L. Hua, and A. Kartavtseff, 2008: Variability at intermediate depths at the equator in the Atlantic Ocean in 2000–06: Annual cycle, equatorial deep jets, and intraseasonal meridional velocity fluctuations. *J. Phys. Oceanogr.*, **38**, 1794–1806, https://doi.org/10.1175/2008JPO3781.1.

Cane, M. A., and E. S. Sarachik, 1977: Forced baroclinic ocean motions: II. The linear equatorial bounded case. *J. Mar. Res.*, **35**, 395–432.

——, and D. W. Moore, 1981: A note on low-frequency equatorial basin modes. *J. Phys. Oceanogr.*, **11**, 1578–1584, https://doi.org/10.1175/1520-0485(1981)011<1578:ANOLFE>2.0.CO;2.

Claus, M., R. J. Greatbatch, and P. Brandt, 2014: Influence of the barotropic mean flow on the width and the structure of the Atlantic equatorial deep jets. *J. Phys. Oceanogr.*, **44**, 2485–2497, https://doi.org/10.1175/JPO-D-14-0056.1.

——, ——, ——, and J. M. Toole, 2016: Forcing of the Atlantic equatorial deep jets derived from observations. *J. Phys. Oceanogr.*, **46**, 3549–3562, https://doi.org/10.1175/JPO-D-16-0140.1.

Crameri, F., 2018: Scientific colour maps. Zenodo, accessed 9 April 2021, https://doi.org/10.5281/zenodo.1243862.

Cravatte, S., W. S. Kessler, and F. Marin, 2012: Intermediate zonal jets in the tropical Pacific Ocean observed by Argo floats. *J. Phys. Oceanogr.*, **42**, 1475–1485, https://doi.org/10.1175/JPO-D-11-0206.1.

——, E. Kestenare, F. Marin, P. Dutrieux, and E. Firing, 2017: Subthermocline and intermediate zonal currents in the tropical Pacific Ocean: Paths and vertical structure. *J. Phys. Oceanogr.*, **47**, 2305–2324, https://doi.org/10.1175/JPO-D-17-0043.1.

Delpech, A., S. Cravatte, F. Marin, C. Ménesguen, and Y. Morel, 2020a: Deep eddy kinetic energy in the tropical Pacific from Lagrangian floats. *J. Geophys. Res. Oceans*, **125**, e2020JC016313, https://doi.org/10.1029/2020JC016313.

——, ——, ——, Y. Morel, E. Gronchi, and E. Kestenare, 2020b: Observed tracer fields structuration by middepth zonal jets in the tropical Pacific. *J. Phys. Oceanogr.*, **50**, 281–304, https://doi.org/10.1175/JPO-D-19-0132.1.

——, C. Ménesguen, Y. Morel, L. N. Thomas, F. Marin, S. Cravatte, and S. Le Gentil, 2021: Intra-annual Rossby waves destabilization as a potential driver of low-latitude zonal jets: Barotropic dynamics. *J. Phys. Oceanogr.*, **51**, 365–384, https://doi.org/10.1175/JPO-D-20-0180.1.

d'Orgeville, M., B. L. Hua, and H. Sasaki, 2007: Equatorial deep jets triggered by a large vertical scale variability within the western boundary layer. *J. Mar. Res.*, **65**, 1–25, https://doi.org/10.1357/002224007780388720.

Efron, B., 1979: The 1977 Rietz Lecture. Bootstrap methods: Another look at the jackknife. *Ann. Stat.*, **7**, 1–26, https://doi.org/10.1214/aos/1176344552.

Eriksen, C. C., 1982: Geostrophic equatorial deep jets. *J. Mar. Res.*, **40**, 143–157.

Gill, A. E., 1982: *Atmosphere–Ocean Dynamics.* International Geophysics Series, Vol. 30, Academic Press, 62 pp.

Gouriou, Y., B. Bourlès, H. Mercier, and R. Chuchla, 1999: Deep jets in the equatorial Atlantic Ocean. *J. Geophys. Res.*, **104**, 21 217–21 226, https://doi.org/10.1029/1999JC900057.

——, and Coauthors, 2001: Deep circulation in the equatorial Atlantic Ocean. *Geophys. Res. Lett.*, **28**, 819–822, https://doi.org/10.1029/2000GL012326.

Greatbatch, R. J., P. Brandt, M. Claus, S.-H. Didwischus, and Y. Fu, 2012: On the width of the equatorial deep jets. *J. Phys. Oceanogr.*, **42**, 1729–1740, https://doi.org/10.1175/JPO-D-11-0238.1.

——, and Coauthors, 2018: Evidence for the maintenance of slowly varying equatorial currents by intraseasonal variability. *Geophys. Res. Lett.*, **45**, 1923–1929, https://doi.org/10.1002/2017GL076662.

Hayes, S. P., and H. B. Milburn, 1980: On the vertical structure of velocity in the eastern equatorial Pacific. *J. Phys. Oceanogr.*, **10**, 633–635, https://doi.org/10.1175/1520-0485(1980)010<0633:OTVSOV>2.0.CO;2.

Hua, B. L., M. d'Orgeville, M. D. Fruman, C. Ménesguen, R. Schopp, P. Klein, and H. Sasaki, 2008: Destabilization of mixed Rossby gravity waves and the formation of equatorial zonal jets. *J. Fluid Mech.*, **610**, 311–341, https://doi.org/10.1017/S0022112008002656.

Hunter, J. D., 2007: Matplotlib: A 2D graphics environment. *Comput. Sci. Eng.*, **9**, 90–95, https://doi.org/10.1109/MCSE.2007.55.

Jayne, S. R., D. Roemmich, N. Zilberman, S. C. Riser, K. S. Johnson, G. C. Johnson, and S. R. Piotrowicz, 2017: The Argo program: Present and future. *Oceanography*, **30**, 18–28, https://doi.org/10.5670/oceanog.2017.213.

Johnson, G. C., and D. Zhang, 2003: Structure of the Atlantic Ocean equatorial deep jets. *J. Phys. Oceanogr.*, **33**, 600–609, https://doi.org/10.1175/1520-0485(2003)033<0600:SOTAOE>2.0.CO;2.

——, E. Kunze, K. E. McTaggart, and D. W. Moore, 2002: Temporal and spatial structure of the equatorial deep jets in the Pacific Ocean. *J. Phys. Oceanogr.*, **32**, 3396–3407, https://doi.org/10.1175/1520-0485(2002)032<3396:TASSOT>2.0.CO;2.

Leaman, K. D., and T. B. Sanford, 1975: Vertical energy propagation of inertial waves: A vector spectral analysis of velocity profiles. *J. Geophys. Res.*, **80**, 1975–1978, https://doi.org/10.1029/JC080i015p01975.

Lebedev, K. V., H. Yoshinari, N. A. Maximenko, and P. W. Hacker, 2007: YoMaHa'07: Velocity data assessed from trajectories of Argo floats at parking level and at the sea surface. IPRC Tech. Note 4(2), 16 pp., http://apdrc.soest.hawaii.edu/projects/yomaha/.

Leetmaa, A., and P. F. Spain, 1981: Results from a velocity transect along the equator from 125° to 159°W. *J. Phys. Oceanogr.*, **11**, 1030–1033, https://doi.org/10.1175/1520-0485(1981)011<1030:RFAVTA>2.0.CO;2.

Lomb, N. R., 1976: Least-squares frequency analysis of unequally spaced data. *Astrophys. Space Sci.*, **39**, 447–462, https://doi.org/10.1007/BF00648343.

Luyten, J. R., and J. C. Swallow, 1976: Equatorial undercurrents. *Deep-Sea Res. Oceanogr. Abstr.*, **23**, 999–1001, https://doi.org/10.1016/0011-7471(76)90830-5.

Matthießen, J.-D., R. J. Greatbatch, P. Brandt, M. Claus, and S.-H. Didwischus, 2015: Influence of the equatorial deep jets on the north equatorial countercurrent. *Ocean Dyn.*, **65**, 1095–1102, https://doi.org/10.1007/s10236-015-0855-5.

——, ——, M. Claus, F. Ascani, and P. Brandt, 2017: The emergence of equatorial deep jets in an idealised primitive equation model: An interpretation in terms of basin modes. *Ocean Dyn.*, **67**, 1511–1522, https://doi.org/10.1007/s10236-017-1111-y.

Ménesguen, C., A. Delpech, F. Marin, S. Cravatte, F. Schopp, and Y. Morel, 2019: Observations and mechanisms for the formation of deep equatorial and tropical circulation. *Earth Space Sci.*, **6**, 370–386, https://doi.org/10.1029/2018EA000438.

Ponte, R. M., J. Luyten, and P. L. Richardson, 1990: Equatorial deep jets in the Atlantic Ocean. *Deep-Sea Res.*, **37A**, 711–713, https://doi.org/10.1016/0198-0149(90)90100-A.

Scargle, J. D., 1982: Studies in astronomical time series analysis. II. Statistical aspects of spectral analysis of unevenly spaced data. *Astrophys. J.*, **263**, 835–853, https://doi.org/10.1086/160554.

Schopf, P. S., D. L. T. Anderson, and R. Smith, 1981: Beta-dispersion of low-frequency Rossby waves. *Dyn. Atmos. Oceans*, **5**, 187–214, https://doi.org/10.1016/0377-0265(81)90011-7.

Tuchen, F. P., P. Brandt, M. Claus, and R. Hummels, 2018: Deep intraseasonal variability in the central equatorial Atlantic. *J. Phys. Oceanogr.*, **48**, 2851–2865, https://doi.org/10.1175/JPO-D-18-0059.1.

Youngs, M. K., and G. C. Johnson, 2015: Basin-wavelength equatorial deep jet signals across three oceans. *J. Phys. Oceanogr.*, **45**, 2134–2148, https://doi.org/10.1175/JPO-D-14-0181.1.